A Film-Cooling Correlation for Shaped Holes on a Flat-Plate Surface

Will F. Colban
Combustion Research Facility,
Sandia National Laboratories,
Livermore, CA 94551

Karen A. Thole
Department of Mechanical and Nuclear Engineering,
Pennsylvania State University,
University Park, PA 16802

David Bogard
Department of Mechanical Engineering,
University of Texas at Austin,
Austin, TX 78712

A common method of optimizing coolant performance in gas turbine engines is through the use of shaped film-cooling holes. Despite widespread use of shaped holes, existing correlations for predicting performance are limited to narrow ranges of parameters. This study extends the prediction capability for shaped holes through the development of a physics-based empirical correlation for predicting laterally averaged film-cooling effectiveness on a flat-plate downstream of a row of shaped film-cooling holes. Existing data were used to determine the physical relationship between film-cooling effectiveness and several parameters, including blowing ratio, hole coverage ratio, area ratio, and hole spacing. Those relationships were then incorporated into the skeleton form of an empirical correlation, using results from the literature to determine coefficients for the correlation. Predictions from the current correlation, as well as existing shaped-hole correlations and a cylindrical hole correlation, were compared with the existing experimental data. Results show that the current physics-based correlation yields a significant improvement in predictive capability, by expanding the valid parameter range and improving agreement with experimental data. Particularly significant is the inclusion of higher blowing ratio conditions (up to $M=2.5$) into the current correlation, whereas the existing correlations worked adequately only at lower blowing ratios ($M \approx 0.5$).
[DOI: 10.1115/1.4002064]

1 Introduction

Demands for increased power output from gas turbine engines and decreased fuel consumption have caused engine designers to increase combustion exit gas temperatures, which in turn leads to a rise in efficiency and increased power output following from analysis of the Brayton cycle. Cooling the exposed combustor and downstream turbine surfaces has subsequently become a critical issue because of increased thermal loads, with external film-cooling being a particularly significant topic. Because film-cooling uses bleed air from high-pressure stages in the compressor, the use of more coolant lowers the overall engine efficiency by reducing the core mass flow. Additionally, pumping losses are also increased with higher coolant flow. Clearly there is a trade-off, and the goal of film-cooling engine designers has been to reduce the amount of coolant used, while at the same time increasing the cooling efficiency. One approach to increase coolant efficiency is to alter the geometry of a film-cooling hole from a standard cylindrical shape to one with a diffused exit shape. There are a number of variations of the shaped cooling hole, but perhaps the most common varieties are the fan-shaped (laterally expanded) and the laidback fan-shaped (fully expanded) hole. The fan-shaped features an expansion in the lateral direction, while the laidback fan-shaped hole includes an additional forward expansion.

Goldstein et al. [1] first showed the benefits of shaped-hole cooling over round holes. Their flow visualization studies showed that coolant exiting a fan-shaped hole stays attached to the surface at a much higher blowing ratio than for a round hole. By expanding the jet as it exits the hole, the effective momentum at the ejection location is reduced. The reduced jet momentum in turn allows the coolant to remain attached to the surface, providing more efficient cooling. An additional benefit of fan-shaped cooling noted by Goldstein et al. [1] is increased lateral spreading, resulting in coolant distribution over a larger surface area.

Cooling schemes in current gas turbine engines are extremely complex, requiring a large effort and much iteration to design [2]. Additionally, three-dimensional finite element analysis (FEA) and computational fluid dynamics (CFD) predictions are costly and time intensive, especially when the location of cooling holes and other cooling features changes from iteration to iteration. For this reason, empirical correlations for information such as film-cooling effectiveness and heat transfer coefficients are an essential tool for engine designers.

There has been a number of film-cooling effectiveness correlations published for cylindrical cooling holes. However, despite the extensive use of fan-shaped holes in industry, there have been no definitive correlations published for shaped holes, although some commonly used skeleton correlations—where the coefficients are determined from data—are suggested by Bunker [2]. A number of fan-shaped-hole studies currently exist in the open literature, examining the effects of blowing ratio, momentum ratio, density ratio, turbulence intensity, surface angle, lateral expansion angle, forward expansion angle, hole spacing, coverage, area ratio, entrance length, and the approaching boundary layer. This study has taken available data sets from the open literature, as well as an unpublished data set contributed by one of the co-authors, and developed a correlation for laterally averaged adiabatic film-cooling effectiveness downstream of a single row of fan-shaped holes with low freestream turbulence and a negligible freestream pressure gradient. The goal of the correlation was to encompass as large a range as possible of certain relevant parameters, as determined from an analysis of the available literature. Based on a survey of the effects of relevant film-cooling parameters from the literature, the following parameters were identified and included into the present correlation; blowing ratio, hole spacing, coverage, and area ratio.

2 Past Studies

Adiabatic film-cooling effectiveness is essentially a nondimensional temperature, defined as

Contributed by the International Gas Turbine Institute (IGTI) of ASME for publication in the JOURNAL OF TURBOMACHINERY. Manuscript received August 28, 2008; final manuscript received June 4, 2010; published online September 7, 2010. Editor: David Wisler.

$$\eta(X,Z) = \frac{T_{ad}(X,Z) - T_{jet}}{T_\infty - T_{jet}} \quad (1)$$

where $T_{ad}(x,y)$ is the adiabatic surface temperature, T_{jet} is the jet coolant temperature, and T_∞ is the freestream temperature. Together with the heat transfer coefficient, one can use η to predict metal surface temperatures. Furthermore, η is typically described in terms of laterally averaged η, averaged across the lateral dimension Z:

$$\bar{\eta}(X) = \frac{1}{\Delta Z}\int \eta(X,Z)dZ \quad (2)$$

In the case of a slot, η at the centerline is equivalent to $\bar{\eta}$.

A number of early correlations were derived theoretically (as summarized by Goldstein [3]) for two-dimensional slot film-cooling. The heat sink approach modeled the injected fluid as a heat sink that subsequently lowered the temperature in the downstream boundary layer. A mass and energy balance was then performed on the developing turbulent boundary layer, assuming it was composed of entrained mainstream flow and injected coolant. A turbulent boundary layer profile was then used to predict the amount of entrained freestream gas at a given location downstream. Heat sink models all yielded equations for film-cooling effectiveness of the form

$$\bar{\eta} = \frac{C_1}{C_2 + C_3\xi^{0.8}} \quad (3)$$

where C_1, C_2, and C_3 are some combination of constants and fluid properties (depending on the particular development), and ξ is a distance scaling parameter of the form

$$\xi = \left(\frac{X}{MS_e}\right)\left[\frac{\mu_2}{\mu_\infty}\mathrm{Re}_2\right]^{-0.25} \quad (4)$$

The heat sink models did not include any consideration for how the coolant affected the velocity boundary layer, such as thickening and separation. Those models were also meant for two-dimensional, continuous, tangential slot injection, which has a fundamentally different interaction with the mainstream gas than inclined discrete hole injection. In general, two-dimensional heat sink models typically overpredict film-cooling effectiveness for discrete holes, especially in the near-hole region ($X/D < 10$) and at higher blowing ratios.

The heat sink model was also applied to three-dimensional film-cooling injection through a single discrete hole by Ramsey et al. [4], giving the following equation for film-cooling effectiveness,

$$\eta(X,Z) = \frac{MU_\infty D}{8\varepsilon(X/D + 0.5)}\exp\left[-0.693\left(\frac{Z}{Z_{1/2}}\right)^2\right] \quad (5)$$

This model gives the temperature distribution in both the streamwise and lateral directions. Again, as with other heat sink models, the three-dimensional model performs well only at low blowing ratios where there is no jet lift-off. This model performs poorly for predicting effectiveness for more than one hole if the hole spacing is small enough such that adjacent jet interaction occurs.

An experimentally developed correlation for a single row of cylindrical holes based on blowing ratio and hole geometry was presented by L'Ecuyer and Soechting [5]. In the development of their correlation, they defined three separate flow regimes based on the flow rate through the hole; the mass addition regime, the mixing regime, and the penetration regime. The mass addition regime was characterized by increased effectiveness due to an increase in thermal capacity. The mixing regime was characterized by a trade-off between added thermal capacity and increased coolant/freestream mixing and penetration. The penetration regime was dominated by excessive penetration and subsequent thermal diffusion of the coolant resulting from the large amount of turbulent mixing. The injection angle was determined to affect the onset of transition into the penetration regime, but did not have an effect on the decay of effectiveness, which was determined to be proportional to the following expression far downstream of the hole,

$$\bar{\eta} \propto \left(\frac{X}{MS_e}\right)^{-0.5} \quad (6)$$

Paramount to the development of the model by L'Ecuyer and Soechting [5] was the location of the peak level of film-effectiveness. The peak level of effectiveness occurs at the ejection location in the mass addition regime. However, for the mixing and penetration regimes, wherein jet separation normally occurs, this location occurs at some distance downstream, with the location dependent on the blowing ratio. L'Ecuyer and Soechting [5] used a constant thermal diffusivity model (moving energy sink solution) to accurately predict effectiveness behavior in the mass addition and mixing regimes. A decaying thermal diffusivity model was developed that handled the penetration regime. This correlation has been shown to work well in the mass addition and mixing regimes, although larger uncertainties have been noted in the penetration regime because of insufficient data from the literature.

Baldauf et al. [6] also presented a correlation for streamwise oriented cylindrical holes on a flat plate to predict laterally averaged film-cooling effectiveness at a given downstream distance. They split the flow interaction into two regions: a near ejection region where the coolant behaves as a single jet and a region further downstream dominated by adjacent jet interaction. Again, the concept of a location of maximum effectiveness, which may or may not be at the ejection location depending on the blowing ratio, was used in the correlation development. The correlation presented by Baldauf et al. [6] was rather extensive and included the effects of blowing ratio, momentum flux ratio, turbulence intensity, surface angle, and hole spacing. Overall, this correlation works well for cylindrical hole injection.

The behavior of fan-shaped film-cooling holes has been shown in the literature to be fundamentally different than that of cylindrical holes. Shaped holes on flat plates with negligible freestream pressure gradient do not undergo separation until they reach a blowing ratio of between 3 and 4, at which point a narrowing of the coolant footprint is seen on the surface, but the peak effectiveness still occurs at the hole exit location. The current study attempts to draw parallel between the public fan-shaped data sets and develop a unique physics-based correlation for laterally averaged adiabatic film-cooling effectiveness for fan-shaped holes.

3 Discussion of Relevant Parameters

An excellent review of relevant parameters affecting shaped-hole film-cooling is offered by Bunker [7]. For the development of the correlation presented in this study, a number of those parameters are discussed and evaluated in Secs. 3.1–3.8. Based on that discussion, several parameters have been excluded from the correlation for reasons ranging from negligible effects within the interested range to insufficient data in the open literature to another parameter offering a better collapse of the data.

3.1 Effect of Blowing Ratio (M). The blowing ratio for a shaped hole is defined in the same manner as for a cylindrical hole, with the jet velocity being taken at the metering area. Equation (7) gives the definition for blowing ratio,

$$M = \frac{\rho_{jet}U_{jet}}{\rho_{ext}U_{ext}} \quad (7)$$

where ρ_{jet} is the coolant density, U_{jet} is the average coolant velocity in the cylindrical entrance length of the hole, ρ_{ext} is the external fluid density, and U_{ext} is the local external velocity at the exit location. It should be pointed out that the effective blowing ratio at the hole exit is defined by Eq. (8),

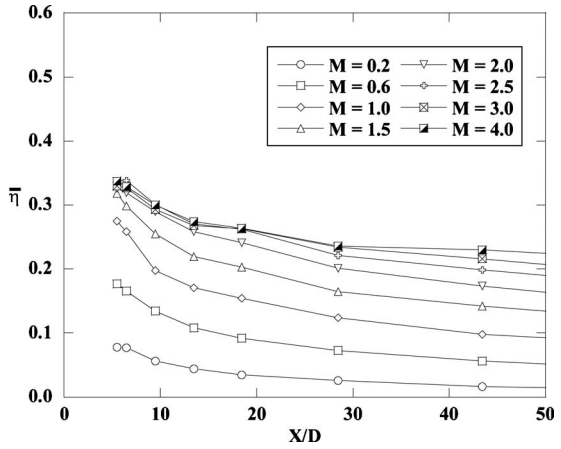

Fig. 1 Effect of blowing ratio on η for shaped holes ($AR=3.9, P/D=6.5, t/P=0.48$) [12]

$$M_{\text{eff,exit}} = M/AR \tag{8}$$

where AR is the cross-sectional area ratio from the hole exit to the hole inlet.

Another parameter similar to blowing ratio, which also deserves mention, is the momentum flux ratio, defined as

$$J = \frac{\rho_{\text{jet}} U_{\text{jet}}^2}{\rho_{\text{ext}} U_{\text{ext}}^2} \tag{9}$$

where J is the ratio of the momentum of the jet relative to the momentum of the freestream gases. In the development of this correlation, both M and J were considered as potential variables. However, the data collapsed much better using M than with J. For this reason, the data reduction in this study has been performed using M, even though J is considered a significant parameter in describing the performance of a film-cooling hole.

As discussed earlier, the behavior of shaped holes differs from that of cylindrical holes. Cylindrical holes yield an increase in film-cooling effectiveness up to a blowing ratio of nearly 0.5 (higher M values for higher density ratios), above which point they begin to separate and the effectiveness decreases with blowing ratio [6]. Figure 1 shows the results from the unpublished shaped-hole data set. Eight blowing ratios ranging from 0.2 to 4.0 are shown for the same hole shape. Clearly, shaped holes do not exhibit the same behavior as cylindrical holes and can sustain increases in effectiveness up to blowing ratios in the range from 3.0 to 4.0. The increase in $\bar{\eta}$ is not proportional, however, to increases in blowing ratio, and is reduced at higher blowing ratios. This dependency suggests a relationship between $\bar{\eta}$ and blowing ratio of the following form:

$$\bar{\eta} \propto M^n \tag{10}$$

where $n<1$ yields a smaller increase in $\bar{\eta}$ for a given $n=0.5$ at higher M.

The other important difference between shaped and cylindrical hole cooling that can be tied to the blowing ratio is the location of peak effectiveness. For cylindrical hole cooling, once the jet separates ($M>0.5$), the location of peak $\bar{\eta}$ migrates downstream from the hole exit location. In contrast, in the conditions considered for this model—flat plate, low freestream turbulence, and negligible freestream pressure gradient—the location of peak $M=1.5$ for shaped-hole cooling is located at the hole exit for a much larger range of M (Fig. 1). Goldstein et al. [1] performed flow visualization for a shaped hole with no freestream flow ($M=\infty$). They showed that while the core of the shaped-hole jet was located slightly off the wall, there was still some cooling that remained attached to the wall, which indicated that total separation did not occur for shaped-hole cooling. This observation simplifies the approach for the correlation, in that it is not necessary to separate the correlation into separate regimes based on peak $\bar{\eta}$ location, such as the methods developed by L'Ecuyer and Soechting [5] and Baldauf et al. [6] for cylindrical holes.

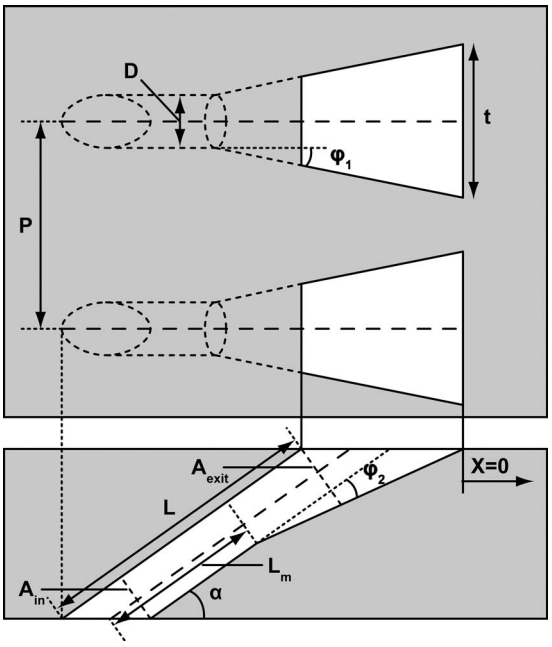

Fig. 2 Illustration of shaped-hole geometrical parameters

3.2 Effect of Downstream Distance (X/D). The relevant geometrical parameters necessary to describe a shaped hole are illustrated in Fig. 2. Not all of the parameters shown in Fig. 2 were accounted for explicitly in the correlation. Some were neglected based on past results, some were not incorporated due to a lack of relevant literature, and some were indirectly incorporated through other parameters. Perhaps the parameter for which the relationship is most obvious is the distance downstream from the hole, nondimensionalized with the hole throat diameter (X/D). As discussed previously, separation is generally not a factor for shaped holes, so the location of peak $\bar{\eta}$ occurs at the hole exit location (indicated in Fig. 2 where $X=0$).

Downstream of the hole, $\bar{\eta}$ is observed to decay according to the following relationship:

$$\bar{\eta} \propto \frac{1}{(X/D)^n} \tag{11}$$

where $n=0.8$ for slot ejection, as shown by Goldstein [3], and $n=0.5$ far downstream of the hole for cylindrical hole cooling, as shown by L'Ecuyer and Soechting [5]. Similarly, the value of n for shaped-hole cooling is expected to lie in the same range.

3.3 Effect of Hole Length (L/D). Figure 3 shows data from the study of Gritsch et al. [8] for three data sets with $L/D=7.5$, 9.5, and 11.5, all with a blowing ratio of $M=1.5$. No difference can be seen among the three data sets in Fig. 3 outside of the experimental uncertainty. The work of Gritsch et al. [8] showed that for shaped holes, the overall length of the hole had essentially no effect on $\bar{\eta}$ in the range $7.5<L/D<11.5$. Perhaps the more relevant length parameter would be the entrance metering length, L_m, because this is the development length for the jet prior to expansion. Lutum and Johnson [9] concluded for cylindrical holes (where $L=L_m$) that the flow development was essentially complete after five hole diameters, showing little effect on performance for $L/D>5$. It is common for a shaped hole to have $L/D>5$, since

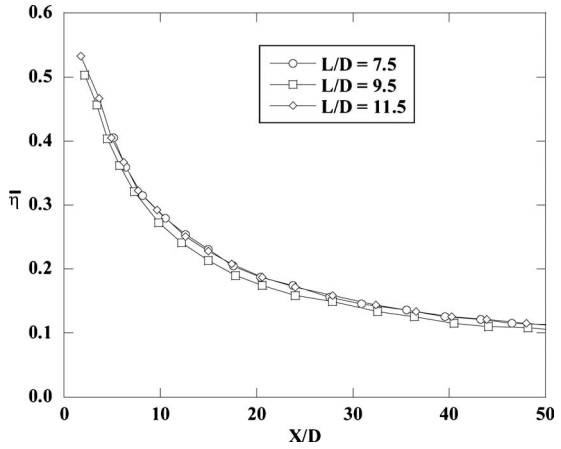

Fig. 3 Effect of L/D ratio on η for shaped holes ($M=1.5, AR=3.5, P/D=6.0, t/P=0.49$) [8]

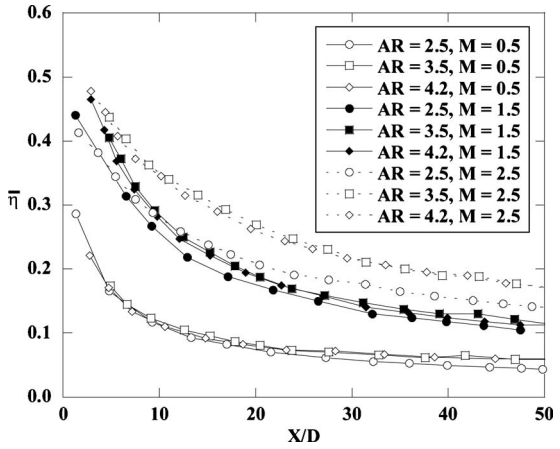

Fig. 4 Effect of area ratio on η for shaped holes ($P/D=6.0, t/P=0.43$) [8]

they are used primarily in situations with shallow surface angles ($\alpha \approx 30$ deg). Furthermore, the data sets considered for the correlation all have $L/D \geq 6$. Therefore, the effect of L/D on $\bar{\eta}$ can be neglected for the development of the correlation.

3.4 Effect of Surface Angle (α). The surface angle of the hole (α) also affects cooling performance. For shallower surface angles, coolant is less likely to migrate away from the surface, increasing cooling efficiency. However, there are two issues with shallower surface angles: machining difficulty and higher pressure losses with increased L/D. The most common surface angle used is 30 deg, with relatively few variations except in the leading edge region on turbine vanes. Furthermore, all of the data used for the correlation development had $\alpha=30$ deg. The correlation has therefore been limited to shaped holes having surface angles of $\alpha=30$ deg.

3.5 Effect of Coverage Ratio (t/P). The ratio of the hole breakout length (t) to the distance between adjacent holes (P) is referred to as the coverage ratio (t/P). Assuming adiabatic conditions and no mixing between adjacent jets, the coverage ratio represents a theoretical limit for maximum $\bar{\eta}$ at the hole exit location ($X/D=0$). The near-hole region typically has the largest conduction errors due to convection inside the hole and is therefore the most difficult region in which to obtain accurate $\bar{\eta}$ data. For this reason, experimental $\bar{\eta}$ values are sometimes greater than t/P at the hole exit. Furthermore, the assumption is also made that the hole is not overly diffused, causing jet separation inside the hole and leading to an effective jet width less than t at the hole exit. Jet separation inside a shaped hole would also promote mixing and lead to $\eta<1$ at the hole exit, an undesirable situation. So in the adiabatic mixing-limited situation where $\eta=1$ across the hole breakout and $\eta=0$ between adjacent holes, the following boundary condition for the correlation must hold:

$$\bar{\eta}(X/D=0)=\frac{t}{P} \tag{12}$$

3.6 Effect of Area Ratio (AR). As described by Bunker [7], there are generally four types of shaped holes: a laterally expanded hole (fan-shaped hole), a forward expanded hole (laidback hole), a laterally and forward expanded hole (laidback fan-shaped hole), and a conically diffused hole. For each of the hole designations, the hole can be defined in terms of the lateral expansion angle (φ_1) and the forward expansion angle (φ_2), as shown in Fig. 2, or in the case of the conically diffused hole, a single expansion angle (φ). The values of these angles depend on the specific application and location of the cooling hole. A general rule-of-thumb is that the expansion angle should not be large enough to yield an overexpanded diffuser, which acts nominally like a separated jet. There is no study available, which offers a systematic examination of the effects of these two expansion angles on the film-cooling performance. However, the combined effect of both expansion angles is intrinsically linked to the more general variable of area ratio.

The area ratio of a shaped hole is given by

$$AR=\frac{A_{\text{exit}}}{A_{\text{in}}} \tag{13}$$

where A_{in} is the cross-sectional inlet area and A_{exit} is the cross-sectional area at the hole exit defined at the leading edge of the hole breakout (illustrated in Fig. 2). The area ratio is a more general way to account for the expansion angles, φ_1 and φ_2, of the shaped hole. It is also important to note that by changing the expansion length of the hole ($L-L_m$), it is possible to have the same expansion angles, φ_1 and φ_2, while having a different AR. Gritsch et al. [8] examined the effects of varying the area ratio of shaped holes, while keeping other relevant parameters constant. Their study described the area ratio as the potential of the geometry to diffuse the coolant and reduce the momentum of the jet exiting the hole. Figure 4 shows some of the results from the study by Gritsch et al. [8] for three area ratios ($AR=2.5$, 3.5, and 4.2) and three blowing ratios ($M=0.5$, 1.5, and 2.5). Figure 4 shows that as M increases, the lowest AR yields lower $\bar{\eta}$. The expectation is that in the limit as AR is reduced to 1, $\bar{\eta}$ will continue to drop until it equals that for cylindrical holes.

3.7 Effect of Hole Spacing (P/D). The nondimensional hole spacing, P/D, is another important parameter that affects $\bar{\eta}$. For large P/D, where there is no hole-to-hole interaction, a closer hole spacing results in an increase in $\bar{\eta}$. Figure 5 shows the results for hole spacings of $P/D=4.0$, 6.0, and 8.0 presented by Gritsch et al. [8] for a blowing ratio of $M=1.5$. As illustrated in Fig. 5, at the same conditions and geometry but for a lower P/D, the resulting $\bar{\eta}$ is higher. The hole coverage ratio (t/P) was the only parameter not maintained for the three cases in Fig. 5 ($0.32<t/P<0.65$). However, t/P has the largest effect in the near-hole region ($X/D<10$), so the difference in $\bar{\eta}$ between the three cases was largely attributable to the hole spacing, P/D. The resulting relationship between P/D and $\bar{\eta}$ is then written as

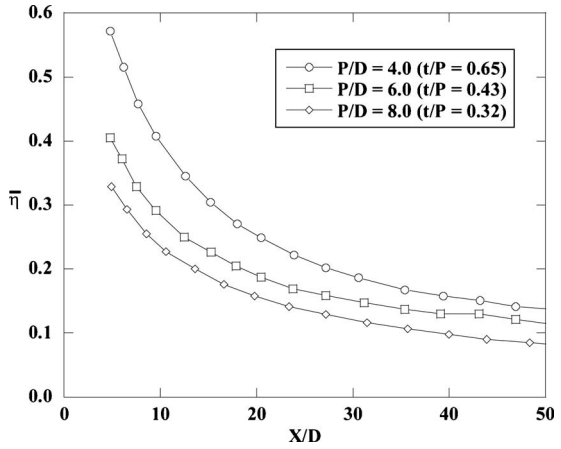

Fig. 5 Effect of hole spacing on η for shaped holes ($M=1.5, AR=4.2$) [8]

$$\bar{\eta} \propto \frac{1}{(P/D)} \tag{14}$$

However, when the hole spacing is reduced to the point where adjacent hole interaction occurs, the additional cooling benefit is no longer strictly inversely proportional to hole spacing, as given by Eq. (14). The data presented by Gritsch et al. [8] suggest that there exists a value for P/D somewhere in the range $4<P/D<6$, below which hole-to-hole interaction occurs and the superposition relationship between $\bar{\eta}$ and P/D would no longer be valid.

3.8 Other Effects. There are several other parameters that affect film-cooling performance. Saumweber et al. [10] showed that freestream turbulence up to 11% has only a marginal effect in reducing film-cooling effectiveness, with decreasing influence for higher blowing ratios. The freestream turbulence level has been left out of the correlation due to the small effect. Additionally, the data used to determine coefficients for the present correlation all had low freestream turbulence levels ($TI=0.2–4.0\%$).

Gritsch et al. [11] showed that film-cooling performance was affected significantly by increasing the external Mach number. Transonic external flow causes a significant alteration of the flow field, resulting in higher effectiveness than the subsonic case. Although higher Mach numbers occur in some regions near turbine vane and endwall surfaces, the present correlation has been limited to subsonic external flow with $\mathrm{Ma}<0.3$.

Density ratio is also known to have an effect on film-cooling performance. However, all of the studies included in the correlation development have engine-representative values (1.7–2.0) and the density ratio is therefore excluded from the correlation.

4 Final Correlation Form

In previous correlations for cylindrical holes, the parameter ξ (given in Eq. (4)) has been used to reduce $\bar{\eta}$. An alternative form of Eq. (4)—not including the effects of viscosity or hole Reynolds number—is given by

$$\xi = \frac{X}{MS_e} \tag{15}$$

with S_e defined as the equivalent slot width for a row of holes. The equivalent slot width is defined as

$$S_e = \frac{A_{\text{exit}}}{P} \tag{16}$$

and is simply the exit area, A_{exit}, divided by the hole spacing, P. It is possible to rewrite Eq. (16) in terms of the nondimensional parameters AR and (P/D),

$$S_e = \frac{\pi D}{4}\frac{AR}{P/D} \tag{17}$$

where the constant $\pi/4$ comes from the substitution of $A_{\text{in}} = \pi/4 \cdot D^2$. Substitution of Eq. (17) into Eq. (15) and rearrangement yield the following definition of ξ in terms of nondimensional parameters,

$$\xi = \frac{4}{\pi}\frac{\frac{X}{D}\frac{P}{D}}{M \cdot AR} \tag{18}$$

The relationships between relevant parameters and $\bar{\eta}$ were discussed in Secs. 2–4. $\bar{\eta}$ was shown to decrease with distance downstream of the hole, X/D. $\bar{\eta}$ increases with M, with the influence growing weaker as M approaches $M=4.0$. $\bar{\eta}$ was also assumed to increase with AR, especially for lower AR up to $AR=3.5$, where Gritsch et al. [8] showed that AR no longer has a noticeable effect on $\bar{\eta}$. The hole spacing, P/D, was shown to have an inverse effect on $\bar{\eta}$, yielding higher $\bar{\eta}$ at lower P/D. Finally, the coverage ratio of the hole, t/P, was chosen as the adiabatic boundary condition for $\bar{\eta}$ at the hole exit, assuming there was no significant mixing within the hole or between adjacent holes. Taking these relationships into account, a predictive correlation for $\bar{\eta}$ can be assumed of the form

$$\bar{\eta} = \frac{1}{P/t + C_1 M^{C_2} \xi^{C_3}} \tag{19}$$

The correlation shown in Eq. (19) reduces to $\bar{\eta}=t/P$ at $X/D=0$. The extra M^{C_2} is included to take into account the fact that the influence of M on $\bar{\eta}$ becomes weaker as M is increased. All of the other nondimensional parameters are included into Eq. (19) such that they affect $\bar{\eta}$ as discussed above. The coefficients C_1, C_2, and C_3 are now determined from existing data sets that incorporate variations in the parameters that have been included into the correlation.

5 Discussion of Data Sets

In all, there were four independent studies from which data were used to determine the coefficients in Eq. (19). As discussed previously, these studies were also used to determine the physical relationships between $\bar{\eta}$ and the different parameters. The four studies were Gritsch et al. [11], Saumweber et al. [10], Gritsch et al. [8], and an unreleased study [12]. Altogether, the studies spanned a range of parameters fairly representative of what would be seen on a turbine airfoil. Table 1 shows the range of parameters encompassed by each study, and gives an idea of the overall scope of the correlation. In all, there were 57 individual data sets included into the correlation development. The ranges of the parameters spanned typical engine values, including $0.2<M<4.0$, $2.50<AR<4.70$, $4.00<P/D<8.00$, and $0.31<t/P<0.75$.

5.1 Data Set 1: Unpublished. The first study, which was taken in 1995, was previously unreleased and contributed by one of the co-authors [12]. The data was taken in the wind tunnel facility at the Turbulence and Turbine Cooling Research Laboratory (TTCRL), which is described in detail by Sinha et al. [13]. Tests were performed in a large-scale, closed-loop wind tunnel on a flat-plate for a single row of holes. The test plate was made from Styrofoam to ensure an adiabatic surface.

The TTCRL data represented eight data sets taken at blowing ratios from 0.2 up to 4.0. The coolant air was cryogenically cooled

Table 1 Range of parameters for each data set

Study	Hole shape	M	α	φ_1	φ_2	AR	P/D	t/P
[12]	LFS	0.2–4.0	30	10	10	3.90	6.5	0.48
[11]	FS	0.5–1.5	30	14	0	3.00	5.5	0.55
	LFS	0.5–1.5	30	14	15	3.10	5.5	0.55
[10]	FS	0.5–2.5	30	14	0	3.00	4.0	0.75
	LFS	0.5–2.5	30	14	15	3.10	4.0	0.75
[8]	LFS	0.5–2.5	30	6	2	3.50	6.0	0.49
	LFS	0.5–2.5	30	7	4	3.50	6.0	0.49
	LFS	0.5–2.5	30	7	11	3.50	6.0	0.49
	LFS	0.5–2.5	30	4	8	4.20	4.0	0.65
	LFS	0.5–2.5	30	4	8	4.20	6.0	0.43
	LFS	0.5–2.5	30	4	8	4.20	8.0	0.32
	LFS	0.5–2.5	30	2	4	2.50	6.0	0.31
	LFS	0.5–2.5	30	4	2	2.50	6.0	0.37
	FS	0.5–2.5	30	4	0	2.50	6.0	0.39
	LFS	0.5–2.5	30	7	2	4.20	6.0	0.57
	FS	0.5–2.5	30	9	0	4.20	6.0	0.63
	LFS	0.5–2.5	30	4	4	3.50	6.0	0.43
	LFS	0.5–2.5	30	8	3	4.70	6.0	0.63

using liquid nitrogen to obtain a density ratio of 2.0. The turbulence intensity at the inlet to the test section was less than 0.3%. The approaching boundary layer was manipulated with a suction and trip wire to match airfoil boundary layer parameters of $\mathrm{Re}_{\delta_2}=360$ and $\delta_2/D=0.045$. Effectiveness measurements were made using an infrared camera, which was calibrated using surface thermocouples.

5.2 Data Set 2: Gritsch et al. The next study that was used to develop the correlation was done by Gritsch et al. [11] and was performed at the Universität Karlsruhe. Adiabatic effectiveness measurements were taken using an infrared camera on a flat plate for a single row of holes. The test plate was made from Tecapek, a high temperature plastic with a low thermal conductivity. The tests were performed in a continuous flow wind tunnel facility, at internal Mach numbers of $\mathrm{Ma}_{\mathrm{in}}=0.0$, 0.3, and 0.6 and external Mach numbers of $\mathrm{Ma}_{\infty}=0.3$, 0.6, and 1.2. However, only the tests performed with $\mathrm{Ma}_{\mathrm{in}}=0.0$ and $\mathrm{Ma}_{\infty}=0.3$ were used for the correlation development. The mainstream turbulence level at the inlet to the test section was less than 2%. Three blowing ratios of $M=0.5$, 1.0, and 1.5 were tested for both fan-shaped and laidback fan-shaped holes.

5.3 Data Set 3: Saumweber et al. Tests by Saumweber et al. [10] were performed using the same geometries and facilities as the study by Gritsch et al. [11]. Three different mainstream inlet turbulence intensities were investigated by Saumweber et al. [10], including $TI=3.6\%$, 7.5%, and 11%, although only the $TI=3.6\%$ case was used for the correlation development. Blowing ratios of $M=0.5$ and 2.5 were reported for fan-shaped and laidback fan-shaped geometries at the low freestream turbulence level. The external Mach number for those tests was $\mathrm{Ma}_{\mathrm{ex}}=0.3$, while the density ratio was $DR=1.7$.

5.4 Data Set 4: Gritsch et al. The final study that was used for the correlation was performed by Gritsch et al. [8]. This was the most extensive study in terms of the range of parameters that were investigated. A total of 16 configurations were tested by Gritsch et al. [8], 13 of which were included in the development of this correlation. Tests were performed in a continuous flow wind tunnel facility on a flat plate for a single row of holes. The holes were machined into a low thermal conductivity polyurethane foam material. Blowing ratios of $M=0.5$, 1.5, and 2.5 were reported for each configuration. All of the tests were run at a density ratio of $DR=1.7$, with an inlet mainstream turbulence intensity of $TI=4\%$, and an external Mach number of $\mathrm{Ma}_{\mathrm{ex}}=0.3$.

6 Correlation Comparisons

6.1 Existing Correlations. In order to determine the efficacy of the current correlation proposed by this study, comparisons were made to existing correlation forms. Four correlation forms were given by Bunker [2] as representative of those used in industry for both cylindrical and shaped holes. These are listed below:

$$\bar{\eta}=\frac{C_1}{\xi^{C_2}} \tag{20}$$

$$\bar{\eta}=\frac{C_1}{C_2+\xi} \tag{21}$$

$$\bar{\eta}=\frac{C_1\ \mathrm{Re}_{\mathrm{jet}}^{0.2}}{\xi^{0.8}} \tag{22}$$

$$\bar{\eta}=\frac{C_1}{1+\xi^{0.8}} \tag{23}$$

where the scaling parameter ξ was defined by Eq. (15). The film-cooling jet Reynolds number, $\mathrm{Re}_{\mathrm{jet}}$, used in Eq. (22) is defined by Eq. (24),

$$\mathrm{Re}_{\mathrm{jet}}=\frac{\rho_{\mathrm{jet}}U_{\mathrm{jet}}S_e}{\mu_{\mathrm{jet}}} \tag{24}$$

The correlation in Eq. (23) as shown by Bunker [2] actually includes an additional coefficient (C_2). However, the correlation matches the data much better by using only the single coefficient. Therefore, the second coefficient has been omitted for the comparison.

The coefficients for each of the correlations mentioned by Bunker [2] were also determined by using the shaped-hole data sets summarized in Table 1. For completeness, the results of the current correlation were also compared with the cylindrical hole correlation of Baldauf et al. [6], just to stress the importance of including the specific hole geometry into the predictive correlation.

Table 2 Linearization of each correlation equation (19)–(23)

Equation	Correlation	Form	Z	X	Y	A	B	C
(19)	$\bar{\eta}=\frac{1}{P/t+C_1M^{C_2}\xi^{C_3}}$	$Z=A+BX+CY$	$\ln\left[\frac{1}{\bar{\eta}}-\frac{P}{t}\right]$	$\ln[M]$	$\ln[\xi]$	$\ln[C_1]$	C_2	C_3
(20) [2]	$\bar{\eta}=\frac{C_1}{\xi^{C_2}}$	$Y=A+BX$	–	$\ln[\xi]$	$\ln[\bar{\eta}]$	$\ln[C_1]$	$-C_2$	–
(21) [2]	$\bar{\eta}=\frac{C_1}{C_2+\xi}$	$Y=A+BX$	–	ξ	$\frac{1}{\bar{\eta}}$	$\frac{C_2}{C_1}$	$\frac{1}{C_1}$	–
(22) [2]	$\bar{\eta}=\frac{C_1\ \mathrm{Re}_{\mathrm{jet}}^{0.2}}{\xi^{0.8}}$	$Y=AX$	–	$\frac{\mathrm{Re}_{\mathrm{jet}}^{0.2}}{\xi^{0.8}}$	$\bar{\eta}$	C_1	–	–
(23) [2]	$\bar{\eta}=\frac{C_1}{1+\xi^{0.8}}$	$Y=AX$	–	$\frac{1}{1+\xi^{0.8}}$	$\bar{\eta}$	C_1	–	–

6.2 Determination of Coefficients for Each Correlation. The determination of the coefficients for each of the five correlations given in Eqs. (19)–(23) was done using the linear regression technique. First, each correlation equation was linearized to either a one variable equation,

$$Y = A + BX \tag{25}$$

or a two variable equation,

$$Z = A + BX + CY \tag{26}$$

The linearization of Eqs. (19)–(23) is summarized in Table 2. The linearized variables, X, Y, and Z were then calculated for each of the 57 data sets. The linearized coefficients A, B, and C were determined using linear regression for either one variable (Eqs. (20)–(23)) or two variables (Eq. (19)). Finally the correlation coefficients C_1, C_2, and C_3 were calculated from the relationships shown in Table 2. A summary of the final correlation coefficients computed based on the data sets is listed in Table 3 for each shaped-hole correlation.

Once the coefficients for each correlation had been determined, it was necessary to determine how well each correlation predicted the available data sets. Values of $\bar{\eta}$ were predicted for each of the 57 data sets using the current correlation in Eq. (19), the four correlations given by Bunker [2] in Eqs. (20)–(23), and the cylindrical hole correlation laid out by Baldauf et al. [6].

The results for two data sets [8] (configuration B at both $M=0.5$ and 2.5), along with the predictions for that blowing ratio and geometry configuration from each correlation, are shown in Figs. 6 and 7. Also listed in Figs. 6 and 7 are the coefficients of determination (R^2) for each correlation prediction. The coefficient of determination is a statistical parameter that shows how much of the variation in the dependent variable is accounted for in the variation of the independent variable(s) by the regression equation or, alternatively, the proportion of the variability in the data that is accounted for by the model. Basically, it is a measure of how well the regression equation predicts the data. The choice of R^2, which describes a well-predicted data set, seems somewhat arbitrary. Indeed, there is no standard value, which is widely accepted, and the degree of acceptability ultimately depends on the application and desired accuracy. For the purpose of this study, R^2 is primarily used to compare the current model to the other pre-existing correlations in terms of wellness-of-fit, not as an overall measure of the model's predictive accuracy. It is simply intended to indicate whether or not the current model has made an improvement in predictive capability. Therefore, a value of $R^2=0.7$ shall be used

Table 3 Correlation coefficients for the correlation equations (19)–(23)

Equation	C_1	C_2	C_3
(19)	0.1721	−0.2664	0.8749
(20) [2]	1.1930	0.5809	–
(21) [2]	5.5605	−8.2863	–
(22) [2]	0.2014	–	–
(23) [2]	2.1200	–	–

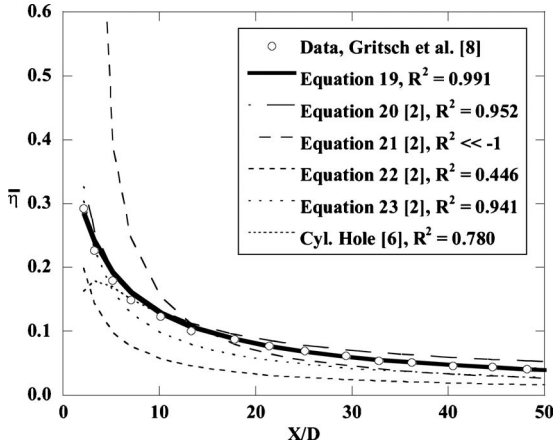

Fig. 6 Correlation predictions versus low blowing ratio data from Gritsch et al. [8] ($M=0.5, AR=3.5, P/D=6.0, t/P=0.49$)

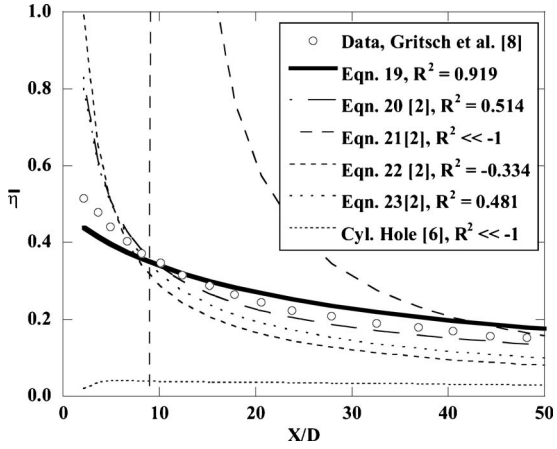

Fig. 7 Correlation predictions versus high blowing ratio data from Gritsch et al. [8] ($M=2.5, AR=3.5, P/D=6.0, t/P=0.49$)

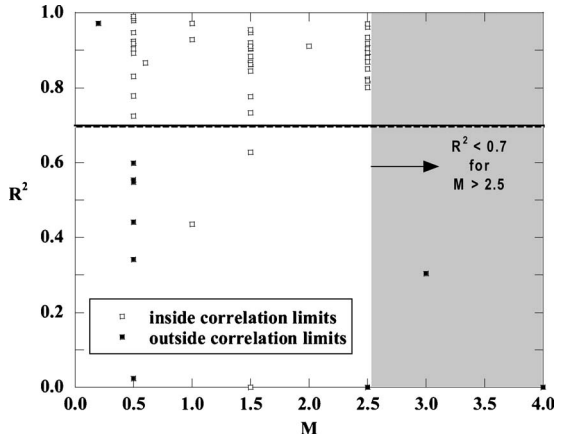

Fig. 8 R^2 values versus blowing ratio for each data set (Eq. (19)). The shaded region indicates the correlation limit for the parameter *M*.

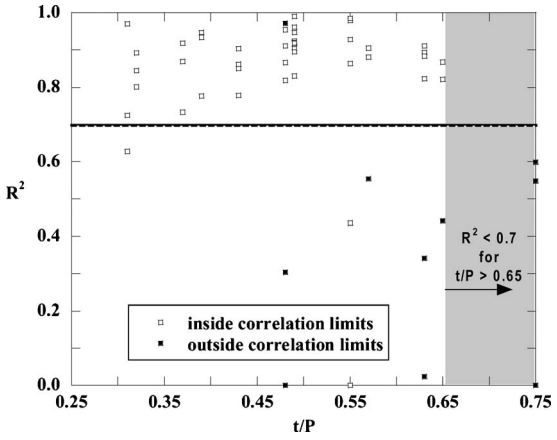

Fig. 9 R^2 values versus coverage ratio for each data set (Eq. (19)). The shaded region indicates the correlation limit for the parameter *t/P*.

as a cut-off value in this study to determine whether or not a data set is well predicted or poorly predicted, and to determine the acceptable parameter ranges for the model.

It is necessary to look at the correlations for both low and high blowing ratios. Figure 6 shows the results of each correlation at $M=0.5$ for geometry configuration B from the study by Gritsch et al. [8]. Altogether, four of the correlations (Eqs. (19), (20), and (23) and Ref. [6]) seem to give good predictions for that particular data set. In fact, if the data for $X/D<10$ is omitted from the R^2 calculation, then R^2 for the Baldauf et al. [6] cylindrical hole correlation is just as good as the current correlation ($R^2=0.988$ compared with $R^2=0.991$). Even the Bunker [2] correlation equation (21) yields a marginal prediction of the data when using only data in the range $X/D>10$ to calculate R^2 ($R^2=0.602$).

Although there seems to be a number of good predictions at low blowing ratios, Fig. 7 shows that there is a much larger discrepancy at high blowing ratios. Figure 7 shows the results of each correlation for the same geometry at a blowing ratio of $M=2.5$. At the high blowing ratio, only the current correlation (Eq. (19)) yields $R^2>0.7$. There are a number of reasons for the poor predictions of the other correlations at the higher blowing ratios with the main reason being that they do not correctly model the physical situation. None of the models proposed by Bunker [2] is constrained by the boundary condition that $\bar{\eta}=t/P$ at $X/D=0$, which is why they all yield a large overprediction in $\bar{\eta}$ as X/D approaches the hole. The cylindrical hole correlation severely underpredicts $\bar{\eta}$ for high blowing ratios, the reason being the fundamental differences in the flow physics for shaped and cylindrical hole cooling. Above $M=0.5$, cylindrical cooling holes exhibit decreases in $\bar{\eta}$, while shaped cooling holes continue to show increases in $\bar{\eta}$ up to blowing ratios of between $M=3$ and 4.

6.3 Correlation Parameter Limits. The final step in determining a film-cooling correlation for shaped holes is to establish the ranges for each nondimensional parameter for which the correlation is valid. Figures 8–10 show the R^2 for all 57 data sets for the current correlation (Eq. (19)) plotted versus the parameters M, t/P, and $AR/(M\cdot P/D)$. The applicable nondimensional parameter ranges for the current correlation were determined by noting which data sets had $R^2<0.7$. For example, in Fig. 8, data sets for which $M>2.5$ all have $R^2<0.7$. Therefore, an upper limit was placed on the parameter M for the current correlation at $M=2.5$. The shaded regions in Figs. 8–10 indicate the limits that were determined for that parameter. All data sets excluded by the shaded regions have been plotted as filled-in symbols in all three figures, meaning that all dark symbols lie outside the limits for at least one parameter. Ultimately, it is desirable to determine nondimensional parameter limits, which would exclude all data sets for which $R^2<0.7$ and include all data sets for which $R^2>0.7$ (note that values for which $R^2<0$ were plotted as $R^2=0$ in Figs. 8–10).

From Fig. 8, it is clear that the current correlation is not valid for $M>2.5$ because for all cases with $M>2.5$, $R^2<0.7$. Similarly, Fig. 9 indicates that for large coverage, $t/P>0.65$, the prediction of the current correlation was not well predicted. Figure 10 shows the R^2 values versus the combination of parameters $AR/(M\cdot P/D)$, which was found to be a particularly limiting combination of nondimensional parameters. Although the point $AR/(M\cdot P/D)=3.0$ has a high R^2 value, Fig. 10 clearly shows most of the R^2 values are less than 0.7 when $AR/(M\cdot P/D)>1.17$.

A similar examination was done for Eqs. (20)–(23) and the cylindrical hole correlation of Baldauf [6]. In order to illustrate how well each correlation did overall for predicting all of the data sets, Figs. 11–15 show R^2 values for each of the Bunker [2] correlations and the Baldauf [6] correlation plotted versus $AR/(M\cdot P/D)$. As compared with the current correlation (Eq. (19)) shown in Fig. 10 where only a relatively few (12 out of 57 total) data sets are below the line indicating $R^2=0.7$, each of the other correlations had a higher number of poorly predicted data sets as illustrated by Figs. 11–15.

Results for the nondimensional parameter limit investigation

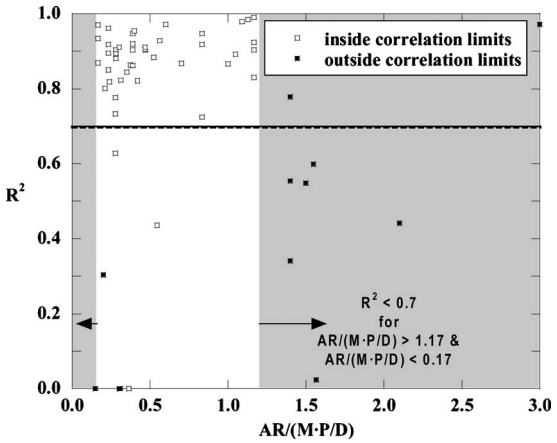

Fig. 10 R^2 values versus the parameter $AR/(M\cdot P/D)$ for each data set (Eq. (19)). The shaded regions indicate the correlation limits for the parameter $AR/(M\cdot P/D)$.

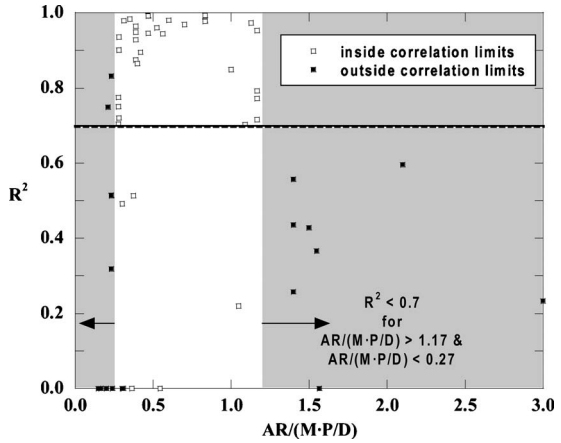

Fig. 11 R^2 values versus the parameter $AR/(M \cdot P/D)$ for each data set (Eq. (20) [2]). The shaded regions indicate the correlation limits for the parameter $AR/(M \cdot P/D)$.

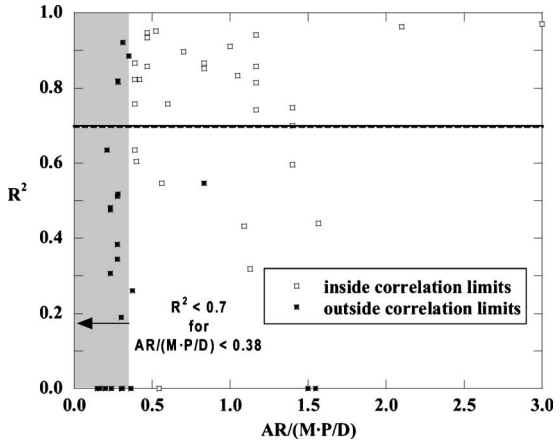

Fig. 14 R^2 values versus the parameter $AR/(M \cdot P/D)$ for each data set (Eq. (23) [2]). The shaded regions indicate the correlation limits for the parameter $AR/(M \cdot P/D)$.

are shown in Table 4 for each correlation equation. Overall, the current correlation equation (Eq. (19)) has the widest ranges on blowing ratio (M) and hole coverage (t/P). Although Eq. (23) has a wider numerical range for $AR/(M \cdot P/D)$ than the current correlation, more of the data sets are clustered in the lower range of $AR/(M \cdot P/D)$ than in the higher range of $AR/(M \cdot P/D)$. For this reason, the number of data sets excluded from the range of $AR/(M \cdot P/D)$ for the current equation (8 data sets) is actually lower than for Eq. (23) (22 data sets). Therefore, the current correlation has the largest overall ranges of applicability across the various nondimensional parameters incorporated into the correlations. Furthermore, the combination of parameter limits suggests that the correlations are not valid for regimes with interaction between adjacent jets, and that the parameter $AR/(M \cdot P/D)$ seems to be a reasonable way to identify the jet interaction regime, when taking $AR/(P/D)$ as a kind of coverage intensity.

In addition to examining the nondimensional parameter limits

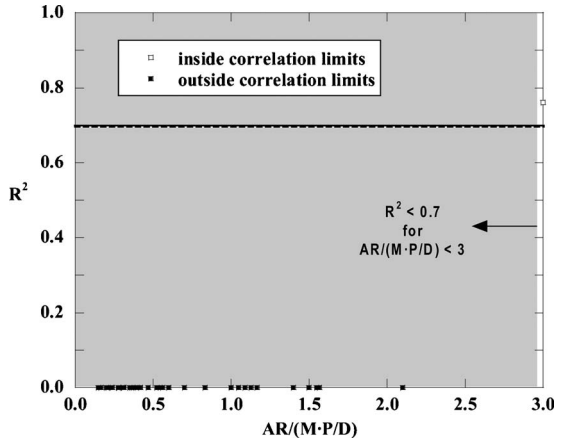

Fig. 12 R^2 values versus the parameter $AR/(M \cdot P/D)$ for each data set (Eq. (21) [2]). The shaded regions indicate the correlation limits for the parameter $AR/(M \cdot P/D)$.

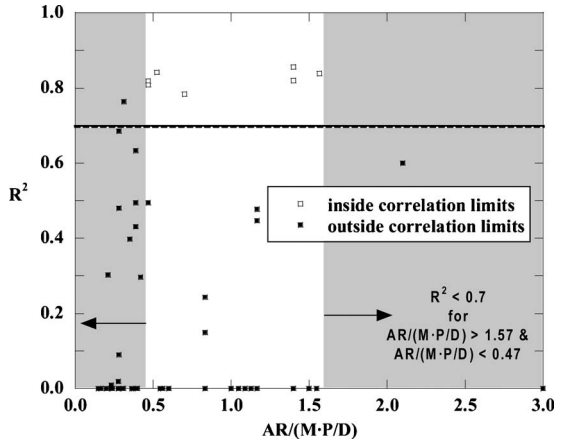

Fig. 13 R^2 values versus the parameter $AR/(M \cdot P/D)$ for each data set (Eq. (22) [2]). The shaded regions indicate the correlation limits for the parameter $AR/(M \cdot P/D)$.

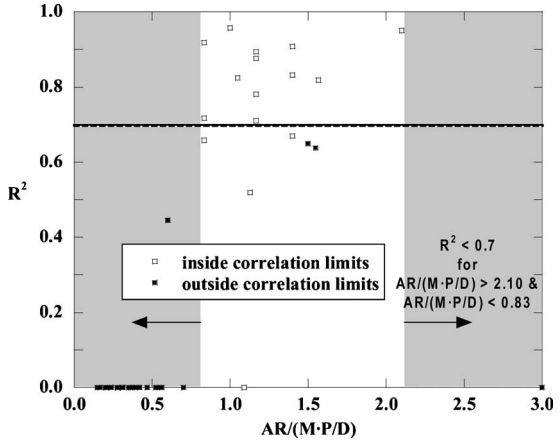

Fig. 15 R^2 values versus the parameter $AR/(M \cdot P/D)$ for each data set (cylindrical hole correlation [6]). The shaded regions indicate the correlation limits for the parameter $AR/(M \cdot P/D)$.

Table 4 Valid shaped-hole parameter limits for each correlation

Equation	M	t/P	$AR/(M \cdot P/D)$
(19)	0.2–2.5	0.31–0.65	0.17–1.17
(20) [2]	0.5–2.5	0.31–0.65	0.27–1.17
(21) [2]	0.2	–	3.0
(22) [2]	0.5–1.5	0.57–0.65	0.47–1.57
(23) [2]	0.2–2.5	0.32–0.65	0.38–3.00
Cyl. hole [6]	0.5–0.6	0.31–0.65	0.83–2.10

Table 5 Valid shaped-hole parameter limits for each correlation

Equation	No. of data sets within limits	Equation prediction within limits (%)
(19)	46	93.5
(20) [2]	36	86.1
(21) [2]	1	100
(22) [2]	7	100
(23) [2]	30	73.3
Cyl. hole [6]	18	67.7

for each correlation, it is useful to examine just how many of the data sets used for developing the correlations fit into the ranges listed in Table 4. Table 5 lists the number of data sets, which fall into the nondimensional parameter limits for each correlation. Table 5 also lists the percentage of those included data sets, which are then well predicted ($R^2 > 0.7$) by that correlation. Ultimately, a good correlation would have a high number of included data sets as well as a high prediction percentage within the assigned limits. The current correlation has the highest number of included data sets, and—aside from Eqs. (21) and (22) which only have 1 and 7 included data sets respectively—it also has the highest prediction percentage.

7 Current Correlation Predictions

It is now necessary to take a closer look at the predictive capability of the current correlation in relation to the relevant nondimensional parameters that were discussed earlier. Figure 16 shows the TTCRL data for blowing ratios of $M=0.6$, 1.5, and 2.5 compared with the predictions from the current correlation. Also listed are the R^2 values, all of which indicate statistically legitimate predictions. The most notable deviation is a slightly higher prediction for low X/D values.

Figure 17 offers a comparison between the current correlation and the data sets for variation in coverage ratio. Overall there was very good agreement, as each prediction had $R^2 > 0.7$. The prediction has been extrapolated to the hole exit to show the boundary condition that $\bar{\eta}=t/P$ at $X/D=0$. In some cases, the data show higher $\bar{\eta}$ values near the hole exit, which was most likely a result of conduction errors associated with the data.

A comparison of the current correlation to data sets with variations in AR is shown in Fig. 18. The correlation matched the AR data from Gritsch et al. [8] well for $X/D > 10$. Notice the slight increase in $\bar{\eta}$ with AR from the correlation on Fig. 18. The dependence of $\bar{\eta}$ on AR was built into the correlation to account for the assumed low AR behavior, even though the results of Gritsch et al. [8] do not show an AR dependence above $AR=3.5$.

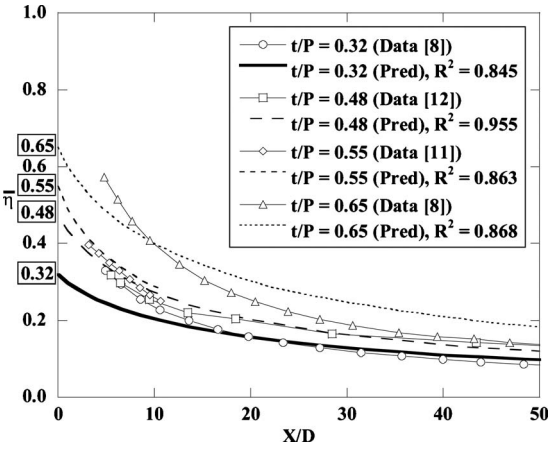

Fig. 17 Comparison of current correlation predictions (Eq. (19)) with experimental data for a range of coverage ratios ($M=1.5$)

Finally, a comparison of the correlation to data from Gritsch et al. [8] for variations of hole spacing is shown in Fig. 19. Once again, the data are well predicted by the model as evidenced by high values of coefficient of determination. The correlation overpredicted $\bar{\eta}$ values for $X/D > 10$ for the closest hole spacing ($P/D < 4$). This was most likely a result of the effect discussed to earlier, whereby adjacent hole interaction occurs for close hole-to-hole spacing, causing an ineffective use of coolant and lowering $\bar{\eta}$. As this effect was not accounted for in the correlation, overprediction of $\bar{\eta}$ is expected for $P/D < 6.0$.

8 Conclusions

The earliest film-cooling correlations were made for continuous slot cooling configurations. The slot correlations were then extrapolated to discrete hole film-cooling with cylindrical holes. Advances in film-cooling technology have led to the extensive use of shaped (noncylindrical exit) holes in turbine applications. Despite the widespread use of shaped holes in industry, an extensive correlation for predicting adiabatic film-cooling effectiveness was not present in the literature, compared with the number of correlations for both slot cooling and cylindrical hole film-cooling. A correla-

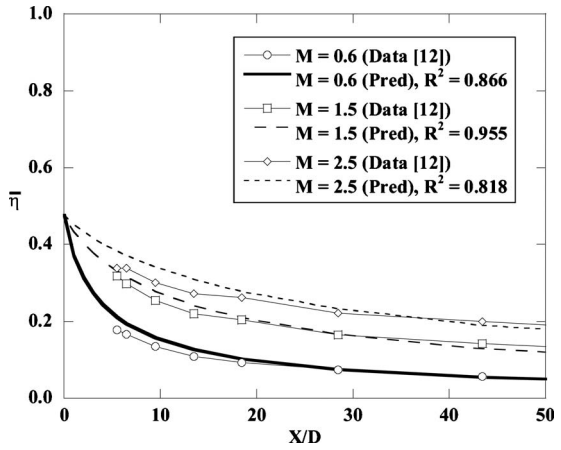

Fig. 16 Comparison of current correlation predictions (Eq. (19)) with experimental data for a range of blowing ratios ($AR=3.9$, $P/D=6.5$, $t/P=0.48$)

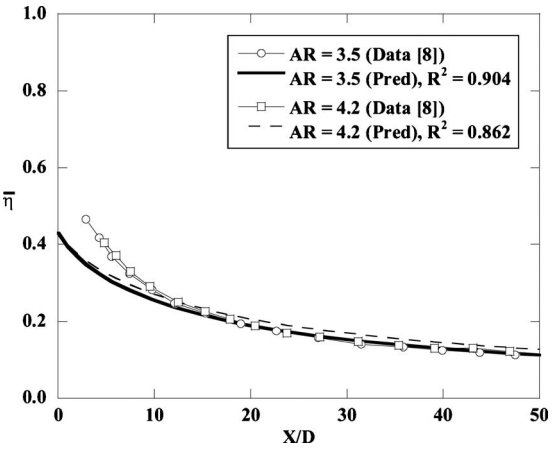

Fig. 18 Comparison of current correlation predictions (Eq. (19)) with experimental data for a range of area ratios ($M=1.5$, $P/D=6.0$, $t/P=0.43$)

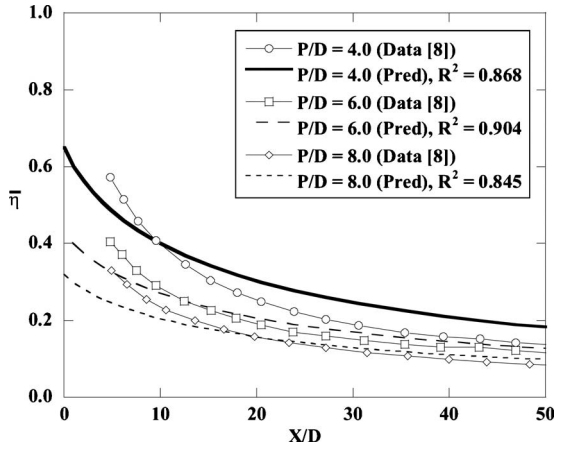

Fig. 19 Comparison of current correlation predictions (Eq. (19)) with experimental data for a range of hole spacings (M=1.5, AR=4.2)

tion for predicting adiabatic film-cooling effectiveness downstream of a single row of shaped holes on a flat-plate surface with low freestream turbulence, an engine-representative density ratio, and a negligible freestream pressure gradient has been developed in this study.

There are fundamental differences in the flow behavior between fan-shaped film-cooling and cylindrical hole injection. Cylindrical hole injection is characterized by jet separation above a blowing ratio of 0.5 and a location of peak film-cooling effectiveness downstream of the hole ejection in the separated regime. Conversely, fan-shaped film-cooling never achieves complete separation, undergoing only partial separation at blowing ratio near and above 3–4.

From examining the results of previous studies, the nondimensional parameters of blowing ratio, area ratio, coverage ratio, and hole spacing were identified as the most relevant to include into the correlation. The correlation that was developed in this study was compared with existing forms that are used in industry, as well as to a cylindrical hole correlation. Based on those comparisons, the current model can be taken as an improvement on the predictive capability for adiabatic film-cooling effectiveness downstream of a row of shaped holes. Additionally, the nondimensional parameter limits for which the previous correlations were valid for shaped holes have been expanded with the current correlation. While many of the existing models offer satisfactory predictions of film-cooling effectiveness at lower blowing ratios (M=0.5), a particular achievement of the current model is the extension to higher blowing ratios (up to M=2.5).

Acknowledgment

The authors would like to acknowledge Mike Blair from Pratt and Whitney for making the data from the TTCRL available for inclusion into this study. Also, the authors are grateful for the advice and direction offered by Michael Gritsch from ALSTOM (Switzerland) Ltd.

Nomenclature

A = cross-sectional area
A, B, C = linearization equation coefficients
AR = area ratio
C = coefficient for the correlation
D = hole throat diameter
DR = density ratio
J = momentum flux ratio
L = length of hole
M = blowing ratio
Ma = Mach number
n = arbitrary exponent
P = hole pitch
R^2 = coefficient of determination
Re = Reynolds number in the metering section of the hole
S = slot width
t = width of hole at trailing edge of hole breakout
T = temperature
TI = turbulence intensity
U = velocity
X = distance downstream of the hole exit
X, Y, Z = linearization equation variables
Z = distance perpendicular to hole centerline

Greek

α = surface inclination angle
δ = boundary layer thickness
η = adiabatic film-cooling effectiveness
μ = dynamic viscosity
ξ = film-cooling scaling parameter
ρ = density
φ = expansion angle for a shaped hole

Subscripts

∞ = freestream conditions
$\frac{1}{2}$ = one-half of the maximum value
1 = lateral expansion angle for a shaped hole
1, 2, 3 = coefficient subscripts
2 = film-cooling jet or forward expansion angle
ad = adiabatic surface
in = the hole inlet location
jet = the coolant jet
e = equivalent (slot width, S)
eff = effective
ext = external
exit = the hole exit location (defined in Fig. 2)
m = metering length

Overbar

– = lateral/pitchwise average

References

[1] Goldstein, R. J., Eckert, E. R. G., and Burggraf, F., 1974, "Effects of Hole Geometry and Density on Three-Dimensional Film Cooling," Heat Mass Transfer, **17**, pp. 595–607.
[2] Bunker, R. S., 2005, "Turbine Cooling Design Analysis," *Gas Turbine Handbook*, Department of Energy, Washington, DC, Sec. 4.2.1.
[3] Goldstein, R. J., 1971, "Film Cooling," Adv. Heat Transfer, **7**, pp. 321–379.
[4] Ramsey, J. W., Goldstein, R. J., and Eckert, E. R. G., 1969, "A Model for Analysis of the Temperature Distribution With Injection of a Heated Jet Into an Isothermal Flow," Paper No. 69-IC-136.
[5] L'Ecuyer, M. R., and Soechting, F. O., 1985, "A Model for Correlating Flat Plate Film-Cooling Effectiveness for Rows of Round Holes," Paper No. AGARD-CP-390.
[6] Baldauf, S., Schleurlen, M., Schulz, A., and Wittig, S., 2002, "Correlation of Film Cooling Effectiveness From Thermographic Measurements at Engine Like Conditions," ASME Paper No. GT-2002–30180.
[7] Bunker, R. S., 2005, "A Review of Shaped Hole Turbine Film-Cooling Technology," ASME J. Heat Transfer, **127**, pp. 441–453.
[8] Gritsch, M., Colban, W., Schär, H., and Döbbeling, K., 2005, "Effect of Hole Geometry on the Thermal Performance of Fan-Shaped Film Cooling Holes," ASME J. Turbomach., **127**, pp. 718–725.
[9] Lutum, E., and Johnson, B. V., 1999, "Influence of the Hole Length-to-Diameter Ratio on Film Cooling With Cylindrical Holes," ASME J. Turbomach., **121**, pp. 209–216.
[10] Saumweber, C., Schulz, A., and Wittig, S., 2003, "Free-Stream Turbulence Effects on Film Cooling With Shaped Holes," ASME J. Turbomach., **125**, pp. 65–73.
[11] Gritsch, M., Schulz, A., and Wittig, S., 1998, "Adiabatic Wall Effectiveness Measurements of Film-Cooling Holes With Expanded Exits," ASME J. Turbomach., **120**, pp. 549–556.
[12] Schmidt, D. L., Sen, B., and Bogard, D. G., 1995, "Effects of Surface Roughness and High Freestream Turbulence on Film Cooling," Report No. TTCRL 95-2.
[13] Sinha, A. K., Bogard, D. G., and Crawford, M. E., 1991, "Gas Turbine Film Cooling: Flowfield Due to a Second Row of Holes," ASME J. Turbomach., **113**, pp. 450–456.